



A novel inorganic–organic nanohybrid material SBA-15@triazine/ $H_5PW_{10}V_2O_{40}$ as efficient catalyst for the one-pot multicomponent synthesis of multisubstituted pyridines

Mohammad Ghanbari¹ · Neda Mollakarimi Dastjerdi¹ · Saman Ahmadi¹ · Sanaz Moradi¹

Received: 14 July 2017 / Accepted: 21 January 2018
© Iranian Chemical Society 2018

Abstract

A novel inorganic–organic nanohybrid material SBA-15@triazine/ $H_5PW_{10}V_2O_{40}$ (SBA-15@ADMPT/ $H_5PW_{10}V_2O_{40}$) was prepared and used as an efficient, eco-friendly, and highly recyclable catalyst for the one-pot multicomponent synthesis of multisubstituted pyridines from the reaction of aldehydes, cyclic ketones, malononitrile, and ammonium acetate with good to excellent yields (77–97%). The nanohybrid catalyst was prepared by the chemical anchoring of Keggin heteropolyacid $H_5PW_{10}V_2O_{40}$ onto the surface of SBA-15 mesoporous silica modified with 2-APTS -4,6-bis(3,5-dimethyl-1H-pyrazol-1-yl)-1,3,5-triazine (ADMPT) linker. Standard characterization data such as FT-IR, XRD, SEM, TEM, BET, EDX, and DTA-TGA spectroscopy confirmed that the heteropolyacid $H_5PW_{10}V_2O_{40}$ is well dispersed on the surface of the solid support and its structure is preserved after immobilization on the SBA-15 mesoporous silica modified with ADMPT. Furthermore, the nanocatalyst can be recovered easily and reused five times without considerable loss of catalytic activity. In general, these advantages highlight this protocol as an attractive and useful methodology, among the other methods reported in the literature, for the eco-friendly and rapid synthesis of biologically active multisubstituted pyridines.

Keywords Nanohybrid catalyst · Heteropolyacid · SBA-15 · $H_5PW_{10}V_2O_{40}$ · Pyridine · Multicomponent reaction

Introduction

Among the nitrogen-containing heterocycles, the pyridine ring system is one of the most prevalent heterocycles found in natural products, medicinal, and functional materials [1–3]. Among these pyridine derivatives, 2-amino-3-cyanopyridine derivatives have been an integral part of molecular skeletons for design of a variety of biologically active compounds. According to their substituents, these compounds have been shown to possess antiviral, antibacterial, and fungicidal activities [4, 5]. 2-Amino-3-cyanopyridine derivatives were also reported as novel IKK- β inhibitors [6], potent inhibitor of HIV-1 integrase [7], and A_{2A} adenosine receptor

antagonists [8]. Due to the importance of 2-amino-3-cyanopyridines, their synthesis has attracted much attention in recent years and many efforts have been made to develop methodologies for the synthesis of 2-amino-3-cyanopyridine derivatives [9–14]. However, most of these procedures suffer from one or more drawbacks such as harsh reaction conditions, long reaction times, use of toxic solvent, expensive transition metal catalyst, operational complexity, and low yields. Therefore, the development of an environmentally benign and practical synthetic route for the efficient preparation of these important pyridine derivatives will be a beneficial and interesting challenge. Furthermore, proposing clean procedures and utilizing eco-friendly and efficient catalysts which can be simply recycled at the end of the reaction have been under permanent attention.

Heteropolyacids (HPAs) are environmentally benign and strong acid catalysts which contain sufficient acidic sites and have been used as prominent catalysts in organic reactions [15–17]. They display high activity and selectivity in organic transformations and allow cleaner processes than conventional catalysts. The major disadvantages of heteropolyacids such as high solubility in aqueous

Electronic supplementary material The online version of this article (<https://doi.org/10.1007/s13738-018-1309-z>) contains supplementary material, which is available to authorized users.

✉ Mohammad Ghanbari
ghanbari-m@kashanu.ac.ir

¹ Department of Organic Chemistry, Faculty of Chemistry, University of Kashan, Kashan 8731753153, Iran

solution, low surface area, and continuous leakage during operation limit the scope of their practical applications. To overcome these limitations, heterogenization of the heteropolyacid through immobilization onto supports, with high surface area, is recommended [18–21]. This strategy enabled the scientists to overcome the restrictions involved in the separation and recycling of the homogeneous catalysts. Typically, the active homogeneous catalyst is supported on inert porous solid materials such as alumina and silica [22], immobilized/anchored on various organic polymers such as resins [23], or encapsulated in the cavities and pores of microporous and mesoporous materials such as zeolites, montmorillonite, MCM-48, MCM-41, and SBA-15 [24].

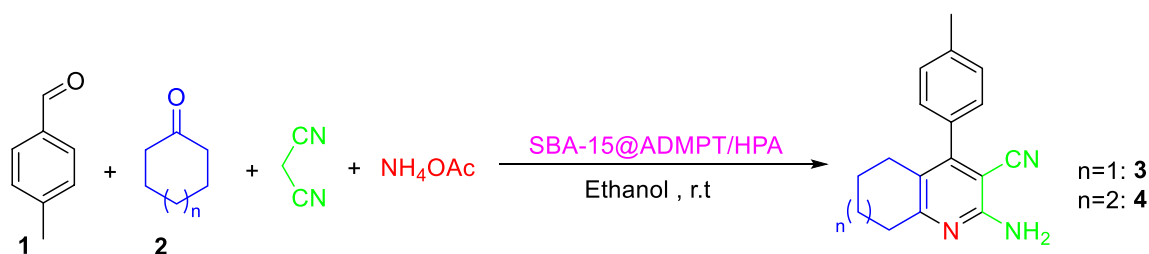
Mesoporous materials have attracted the interest of scientific and industrial societies because of their ability to interact with ions, atoms, and molecules at surfaces, and forming a basis for the preparation of heterogeneous catalysts. Among various mesoporous materials, SBA-15 mesoporous silica with narrow pore size distributions and uniform channels has the ability to accommodate some of the enormous molecules such as heteropolyacids inside the pores, and thus, enable the pore surfaces to be accessed in three dimensions in catalytic reactions [25, 26]. Moreover, SBA-15 shows large specific surface area, high hydrothermal stability, and good adsorption capacity for organic molecules. In addition, mesoporous SBA-15 contains a large number of free silanol groups on its surface which can be modified by reaction with suitable organic modifiers and new inorganic–organic hybrid mesoporous materials can be prepared [27].

As part of our current studies on the development of efficient methods for the preparation of biologically active compounds [28–34], herein, SBA-15@ADMPT/ $H_5PW_{10}V_2O_{40}$ as a new inorganic–organic hybrid mesoporous material was prepared, characterized, and used as an effective catalyst in the synthesis of highly substituted pyridines **3** or **4** via one-pot, four-component reaction of aromatic aldehydes **1**, cyclic ketones **2**, malononitrile, and ammonium acetate at room temperature in ethanol (Scheme 1).

Experimental

Materials

All starting materials used in this work were obtained from Fluka and Merck Chemical Company and were utilized as received without purification. All solvents were dried and distilled under a nitrogen atmosphere prior to use, according to a standard procedure. Thin layer chromatography (TLC) analysis was performed using Silicycle precoated TLC plates (silica gel 60 F₂₅₄). The products were purified by preparative column chromatography on silica gel (0.063–0.200 mm; Merck). FT-IR spectra from 400–4000 cm⁻¹ were recorded on a Perkin–Elmer 781 instrument, using KBr pellets. The NMR spectra were recorded in CDCl₃ and DMSO solvents on a Bruker DRX-400-Advance and Bruker DRX-300-Advance instrument, and INOVA 500 MHz. Chemical shifts were calibrated to the corresponding deuterated solvents. The abbreviations used are singlet (s), doublet (d), triplet (t), and multiplet (m). EI–MS (70 eV): HP 5973 GC–MS instrument; in *m/z*. Thermogravimetric and differential thermal analysis (TGA-DTA) were carried out on a Bahr STA-503 instrument in air at a heating rate of 10 °C min⁻¹. The morphology of the nanostructures was observed on a XL-30 scanning electron microscope (SEM) (Philips, Netherlands). The morphology of the nanostructures was recorded with Philips CM30 transmission electron microscopy (TEM). X-ray powder diffraction analysis (XRD) was performed with Cu-K α radiation on a STADI P diffractometer (STOE, Germany). The elemental analyses were performed on a Flash-1112EA microanalyzer (Thermo Finnigan, Italy). The N₂ adsorption–desorption isotherms and pore characterization were obtained by using a BEL SORB-mini II apparatus at liquid N₂ temperature. In addition, the pore size distributions were calculated by using BJH method from the adsorption branches. Melting points are determined in open capillaries using a Yanagimoto micro-melting point apparatus and are uncorrected. The Keggin heteropolyacid $H_5PW_{10}V_2O_{40}$ was prepared and characterized according to the literature procedure [35].



Scheme 1 General formulation for the synthesis of 2-amino-3-cyanopyridine derivatives

Synthesis

Synthesis of 2-chloro-4,6-bis(3,5-dimethyl-1H-pyrazol-1-yl)-1,3,5-triazine (5)

The 2-chloro-4,6-bis(3,5-dimethyl-1H-pyrazol-1-yl)-1,3,5-triazine **5** was prepared according to our previous reports [36, 37]. Briefly, 0.38 g of 3,5-dimethylpyrazol (4.0 mmol) in 10 mL dry toluene was added dropwise to a solution of cyanuric chloride (0.37 g, 2.0 mmol) and *N,N*-diisopropylethylamine (DIPEA) (0.68 mL, 4.0 mmol) in 40 mL dry toluene at room temperature under nitrogen atmosphere. The mixture was allowed to stir at room temperature overnight. Upon completion (monitoring by TLC), the toluene was removed under reduced pressure, then water was added, and the reaction mixture was stirred for 30 min. The precipitate was filtered, washed with water, air-dried, and was purified by column chromatography. The 2-chloro-4,6-bis(3,5-dimethyl-1H-pyrazol-1-yl)-1,3,5-triazine **5** was obtained as a white solid (Yield 76%). M.p. 146–149 °C; ¹H NMR (CDCl₃, 300 MHz): δ = 2.35 (6H, s, CH₃), 2.76 (6H, s, CH₃), 6.12 (2H, s, CH).

Synthesis of 2-APTS-4,6-bis(3,5-dimethyl-1H-pyrazol-1-yl)-1,3,5-triazine (ADMPT)

ADMPT was prepared according to our previous reports [36, 37]. Briefly, 0.60 g of 2-chloro-4,6-bis(3,5-dimethyl-1H-pyrazol-1-yl)-1,3,5-triazine **5** (2.0 mmol) and 0.34 mL of DIPEA (2.0 mmol) were dissolved in 40 mL dry toluene under nitrogen atmosphere, and the reaction mixture was heated to 80 °C. Then, 0.51 mL of 3-aminopropyltriethoxysilane (APTS) (2.2 mmol) was added dropwise, and the reaction mixture was stirred at 80 °C for 48 h. After this time

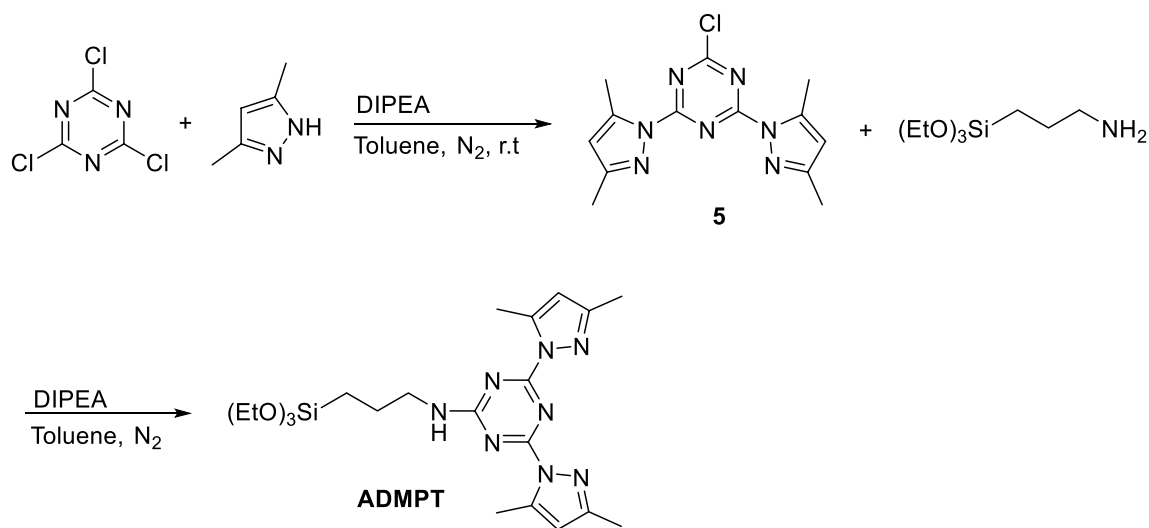
the solvent was removed under reduced pressure, and the product was purified by column chromatography (yield 68%, Scheme 2). M.p. 101–103 °C; ¹H NMR (CDCl₃, 300 MHz): δ = 0.68 (2H, m, CH₂), 1.22 (9H, t, *J* = 7.2 Hz, CH₃), 1.74 (2H, m, CH₂), 2.31 (6H, s, CH₃), 2.70 (3H, s, CH₃), 2.77 (3H, s, CH₃), 3.53 (2H, m, CH₂), 3.82 (6H, q, *J* = 6.9 Hz, CH₃), 6.03 (2H, s, CH).

Synthesis of triazine-functionalized SBA-15 (SBA-15@ADMPT)

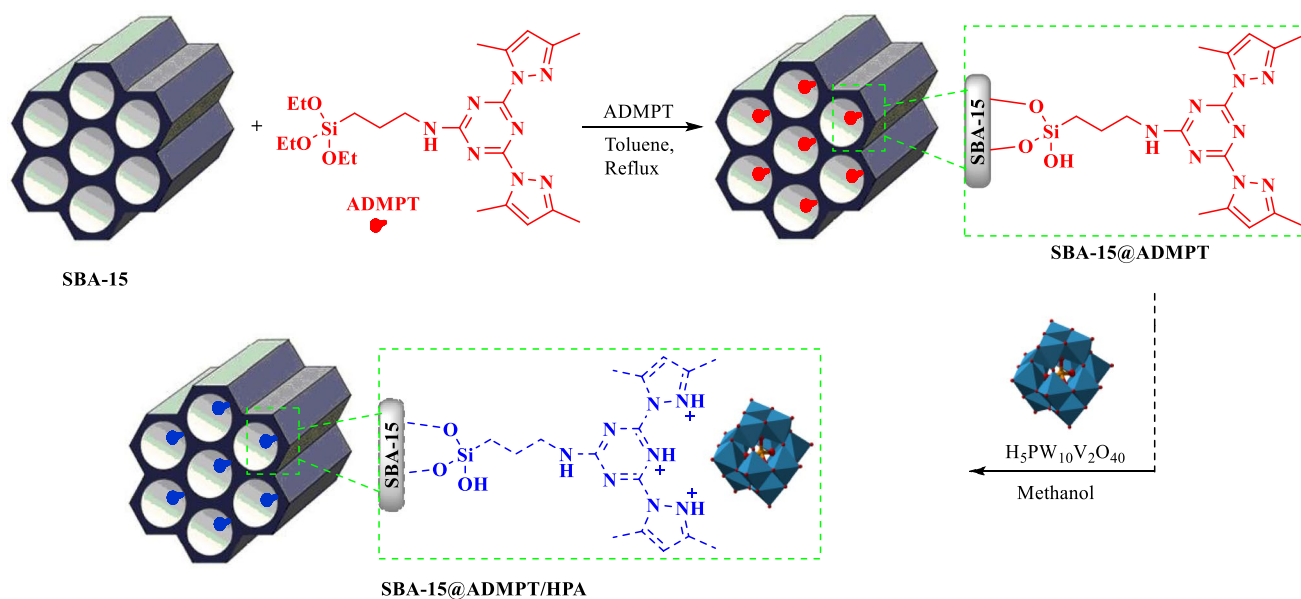
SBA-15 mesoporous silica was prepared according to a previous report [38]. For the preparation of SBA-15@ADMPT, in the first step, 0.5 g of SBA-15 was suspended in 50 ml toluene, and the mixture was stirred for 1 h. Then, 1.46 g of ADMPT was added and the mixture refluxed for 24 h. The white solid was removed by filtration and was washed with toluene, acetone, and ethanol, and then dried at room temperature. FT-IR spectroscopy showed ADMPT anchored onto SBA-15.

Immobilization of H₅PW₁₀V₂O₄₀ on SBA-15@ADMPT (SBA-15@ADMPT/HPA)

For the preparation of SBA-15@ADMPT/HPA, in the first step, 1.0 g of freshly SBA-15@ADMPT was suspended in 50 ml methanol, and then, 0.6 g of H₅PW₁₀V₂O₄₀ was added and the mixture was refluxed for 4 h. The heterogeneous catalyst was separated by filtration and extracted in a Soxhlet extractor using methanol for overnight and thereafter was dried at room temperature (Scheme 3). FT-IR, XRD, and TGA-DTA analysis of SBA-15@ADMPT/HPA catalyst confirmed anchoring of HPA onto the SBA-15@ADMPT. The amount of H₅PW₁₀V₂O₄₀ loading on SBA-15@ADMPT



Scheme 2 Schematic diagram for the synthesis of ADMPT



Scheme 3 Schematic diagram for the preparation of SBA-15@ADMPT/HPA nanocatalyst

was found to be 0.12 mmol g^{-1} , as determined by UV-vis spectroscopy. Furthermore, the SBA-15@ADMPT/HPA did not leach after several hours contact with aqueous solution as confirmed by UV-vis spectroscopy. Therefore, ADMPT linker is a suitable agent for the immobilization process of the heteropolyacid onto the functionalized supporting material. The strong interaction between the SBA-15@ADMPT and $\text{H}_5\text{PW}_{10}\text{V}_2\text{O}_{40}$ made it a suitable heterogeneous catalyst. A schematic representation for the preparation of SBA-15@ADMPT/HPA nanocatalyst is shown in Scheme 3. The scheme shows grafting of ADMPT onto SBA-15 via condensation of hydroxyl and ethoxy groups of the support and linker, respectively; then, the $\text{H}_5\text{PW}_{10}\text{V}_2\text{O}_{40}$ was anchored to SBA-15@ADMPT through electrostatic interaction in the second step.

General procedure for the synthesis of polysubstituted pyridines 3 and 4 catalyzed by SBA-15@ADMPT/HPA nanocatalyst

First, 1 mmol of ketone, 1 mmol of malononitrile, and 1.5 mmol of ammonium acetate were added to 5 mL ethanol solution of aromatic aldehyde (1 mmol) in the presence of 20 mg of the SBA-15@ADMPT/HPA nanocatalyst. The obtained solution was stirred for the required times at room temperature (Table 3). After completion of the reaction, as indicated by TLC using n-hexane/ethyl acetate 4:1 as an eluent, the catalyst was filtered off. Then, the solution is concentrated to give of 2-amino-3-cyanopyridine as crude. This crude product was purified by recrystallization from 95% ethanol to afford pure products 3 or 4. The recovered

SBA-15@ADMPT/HPA nanocatalyst was washed with acetone, dried in air and activated in vacuum oven at 80°C for 2 h, and reused.

Results and discussion

Structural characterization of SBA-15@ADMPT/HPA nanocatalyst

SBA-15 mesoporous silica was modified with triazine by treating with ADMPT in refluxing toluene. The ADMPT was attached to the mesoporous silica surface by condensation of the hydroxyl groups of SBA-15 and the ethoxy groups of ADMPT. The incorporation of the ADMPT on the surface of SBA-15 was confirmed by FT-IR spectrum. Figure 1 shows the FT-IR spectrums of SBA-15@ADMPT/HPA in comparison with SBA-15 and SBA-15@ADMPT. After grafting of ADMPT on the SBA-15 mesoporous, a medium broad band appeared in the range of $2878\text{--}2976 \text{ cm}^{-1}$ (centered at 2930 cm^{-1}), mainly attributed to the C–H stretching vibration, and confirmed graft of ADMPT on the surface of SBA-15. In addition, the appearance of bands at 1602 and 1540 cm^{-1} which attributed to the NH bending and the C=N stretching vibrations, respectively, supports the above conclusion. However, the characteristic band at 3380 cm^{-1} for the NH stretching vibration is covered by the broad stretching vibration band of the adsorbed water molecules in the $3000\text{--}3700 \text{ cm}^{-1}$ region. Furthermore, the Si–O–Si, Si–O, and Si–O–H stretching vibration bands of mesoporous silica appeared at 958 , 1081 , and $3000\text{--}3500 \text{ cm}^{-1}$, respectively.

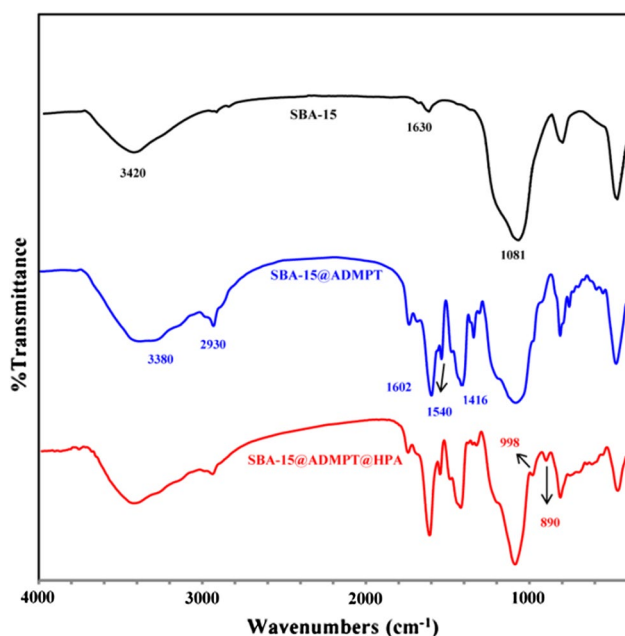


Fig. 1 FT-IR spectra of SBA-15, SBA-15@ADMPT, and SBA-15@ADMPT/HPA

The Keggin heteropolyacid has four characteristic bands in the range of $750\text{--}1100\text{ cm}^{-1}$ [39]. In the literature, the observed peaks at around $778\text{--}784$ and $850\text{--}890\text{ cm}^{-1}$ are assigned to W–O–W. The peaks around $950\text{--}998$ and $1070\text{--}1090\text{ cm}^{-1}$ are related to M=O and P–O bonds, respectively, which clearly indicate the neat structure of Keggin-type heteropolyacid. In the FT-IR spectrum of SBA-15@ADMPT/HPA, these four peaks slightly overlap with SBA-15@ADMPT. However, the new peaks in the spectrum of SBA-15@ADMPT/HPA confirm that loading of HPA was occurred over the SBA-15@ADMPT and $\text{H}_5\text{PW}_{10}\text{V}_2\text{O}_{40}$ was successfully immobilized on the pores of SBA-15 support through strong chemical interaction.

The low-angle XRD patterns of SBA-15, SBA-15@ADMPT, and SBA-15@ADMPT/HPA are shown in Fig. 2. As can be seen the SBA-15 mesoporous displayed three well-resolved peaks, which correspond to reflections (100), (110) and (200) characteristic of two dimensional hexagonal lattice symmetry, as expected for SBA-15-type ordered mesoporous silica [40]. All patterns show an intense reflection (100) at about $2\theta \cong 0.92$, which indicates that the ordered mesoporous structure of SBA-15 remained intact after functionalization with ADMPT and immobilization of $\text{H}_5\text{PW}_{10}\text{V}_2\text{O}_{40}$. An overall decrease in intensity and a slight shift of the characteristic reflection of SBA-15@ADMPT/HPA in low-angle XRD pattern were observed which can be attributed to the lowering local order, such as reduction of scattering contrast between the channel wall and the ligands present on the inner surface of SBA-15. The decrease in the

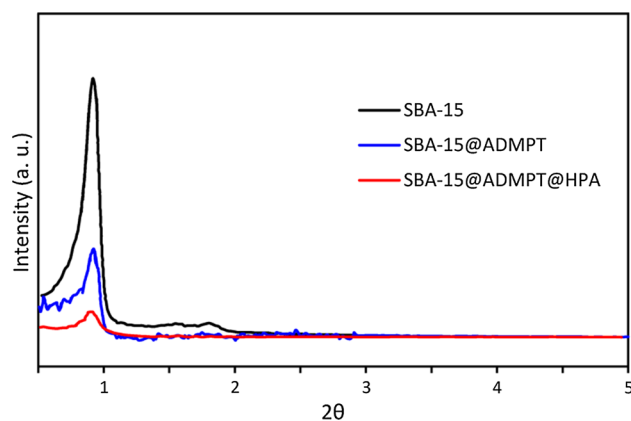


Fig. 2 Low-angle X-ray diffraction patterns of SBA-15, SBA-15@ADMPT, and SBA-15@ADMPT/HPA

intensity of reflections, which is well known in immobilization of various catalysts on mesoporous silicas [41, 42], indicates that the $\text{H}_5\text{PW}_{10}\text{V}_2\text{O}_{40}$ mostly occupied mesoporous channels.

For further characterization, the wide-angle XRD patterns of $\text{H}_5\text{PW}_{10}\text{V}_2\text{O}_{40}$ immobilized on SBA-15@ADMPT was recorded (Fig. 3). It can be seen that the $\text{H}_5\text{PW}_{10}\text{V}_2\text{O}_{40}$ diffraction peaks were collapsed after immobilization on SBA-15@ADMPT and only a broad peak was observed at about 25° , which confirmed $\text{H}_5\text{PW}_{10}\text{V}_2\text{O}_{40}$ was well dispersed onto SBA-15@ADMPT mesopore. This is in accordance with the XRD pattern of heteropolyacids used in other supports [43, 44].

The textural parameters of the prepared samples such as the BET surface area (S_{BET}), the total pore volume (V_{total}), and the pore diameter (D_{BJH}) are summarized in Table 1. According to Table 1, the decrease in the BET surface area, the total pore volume, and BJH pore diameter after the modification indicate the ligand grafting.

The morphology of the SBA-15@ADMPT and SBA-15@ADMPT/HPA was investigated by SEM technique

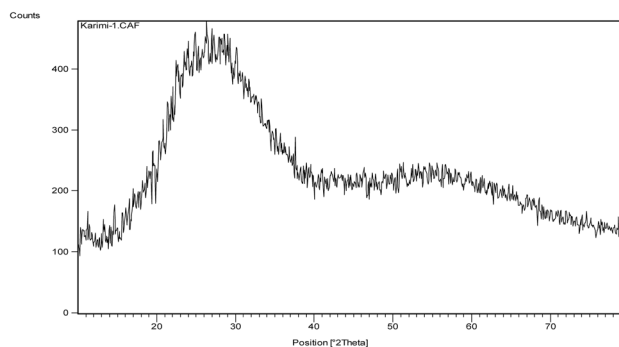


Fig. 3 Wide-angle X-ray diffraction patterns of SBA-15@ADMPT/HPA nanocatalyst

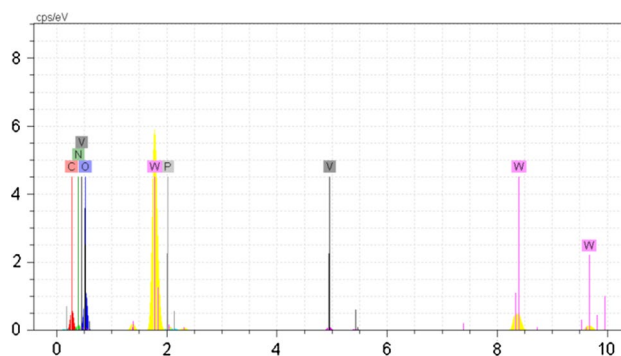
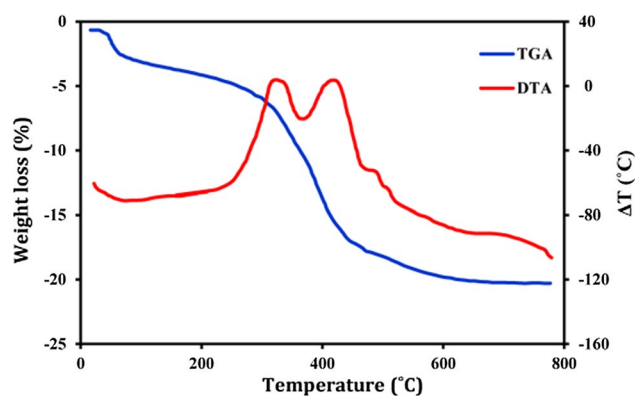
Table 1 Textural and physicochemical properties of prepared compounds

Samples	S_{BET} (m^2/g)	V (cm^3/g)	D_{BJH} (nm)
SBA-15	863	1.040	8.5
SBA-15@ADMPT	451	0.810	8.0
SBA-15@ADMPT/HPA	281	0.396	6.8

as shown in Fig. 4. These micrographs clearly show both materials have similar texture and functionalization with ADMPT and anchoring $\text{H}_5\text{PW}_{10}\text{V}_2\text{O}_{40}$ had no significant effect on the structure of pure SBA-15. Furthermore, the SEM of the SBA-15@ADMPT/HPA clearly shows that the $\text{H}_5\text{PW}_{10}\text{V}_2\text{O}_{40}$ is well dispersed in SBA-15@ADMPT and can be used as a heterogeneous catalyst. On the other hand, the TEM image of SBA-15@ADMPT/HPA (Fig. 4c) reveals the parallel channels, which resemble the pores configuration of SBA-15.

Concerning the chemical composition of the SBA-15@ADMPT/HPA nanocatalyst, EDX analysis was carried out (Fig. 5). The analysis of EDX spectrum proved existence of tungsten, vanadium, nitrogen, carbon, phosphor, and silicon in the nanocatalyst, which confirmed $\text{H}_5\text{PW}_{10}\text{V}_2\text{O}_{40}$ grafted successfully on SBA-15@ADMPT mesoporous silica.

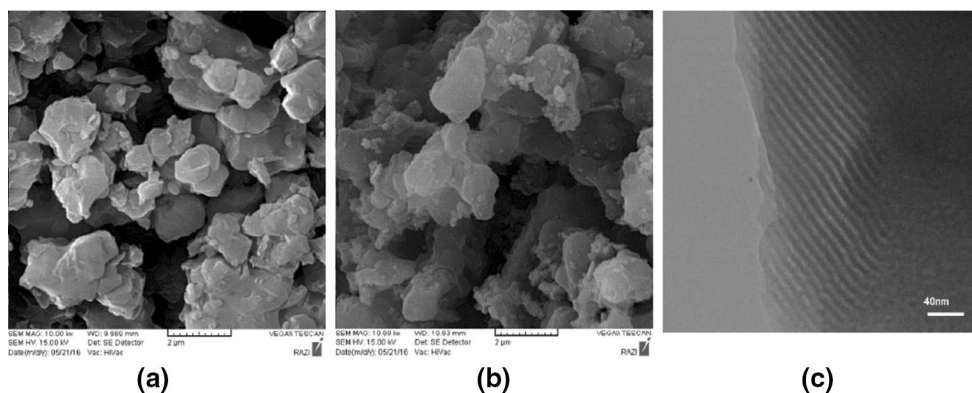
Figure 6 represents the TGA-DTA analysis profile of SBA-15@ADMPT/HPA. The DTA curve profile displayed a broad endothermic peak from room temperature to 220 °C which is associated to the elimination of adsorbed water molecules. The first mass loss step below 100 °C is due to the removal of physically adsorbed water, and the second mass loss in the range of 100–220 °C is attributed with the loss of chemically bonded water molecule or surface silanol condensation. A weight loss occurred in the temperature range of 220–700 °C which is accompanied with exothermic peaks at 324 and 420 °C in the DTA curve, which corresponds to the oxidative decomposition of the organic part

**Fig. 5** EDX spectrum of SBA-15@ADMPT/HPA nanocatalyst**Fig. 6** TGA and DTA curves of SBA-15@ADMPT/HPA

of ADMPT and degradation of the heteropolyacid. Notably, according to thermal analysis, the prepared nanocatalyst was stable up to 280 °C.

Investigation of the catalyst activity

In this study, we have synthesized highly substituted pyridines **3** or **4** via one-pot, four-component reaction of

**Fig. 4** SEM micrograph of **a** SBA-15@ADMPT, and **b** SBA-15@ADMPT/HPA nanocatalyst **c** TEM image of SBA-15@ADMPT/HPA nanocatalyst

aromatic aldehydes **1**, cyclic ketones **2**, malononitrile, and ammonium acetate in the presence of catalytic amounts of the SBA-15@ADMPT/HPA nanocatalyst in ethanol at room temperature. At the outset of our study, to optimize the reaction conditions, a model reaction was carried out by starting from 4-methylbenzaldehyde **1a** (1 mmol), cyclohexanone **2a** (1 mmol), malononitrile (1 mmol), and ammonium acetate (1.5 mmol) in ethanol at room temperature (Scheme 4).

First, the catalytic efficiency of the SBA-15@ADMPT/HPA nanocatalyst was investigated for the preparation of 2-amino-3-cyanopyridine **3a** with various amounts of catalyst (Table 2). In order to evaluate the appropriate amount of catalyst, the model reaction was carried out by using of 15–80 mg of SBA-15@ADMPT/HPA nanocatalyst. According to our results, the best yield was obtained in the presence of 20 mg of SBA-15@ADMPT/HPA nanocatalyst (Table 2, entry 2). As can be seen from Table 2, by increasing the amount of nanocatalyst, the yield of the product was not improved (entry 3 and 4), and also by decreasing it to 15 mg, the desired product was obtained in lower yield (79%) (entry 1).

Table 2 also compares the catalytic activity of SBA-15@ADMPT/HPA nanocatalyst with $H_5PW_{10}V_2O_{40}$, SBA-15@ADMPT, and SBA-15 dispositions, separately, for the synthesis of 2-amino-3-cyanopyridine **3a** under the optimized reaction conditions (entry 5–7). As can be seen, 6.3 mg of $H_5PW_{10}V_2O_{40}$ catalyst led to 54% yield of the desired product after 8 h (entry 5), whereas 20 mg of the SBA-15@ADMPT/HPA nanocatalyst, which includes the same amount of $H_5PW_{10}V_2O_{40}$ (6.3 mg), produced 84% yield of product after a short time of 2 h (entry 2). The modified material SBA-15@ADMPT and unmodified SBA-15 were also catalytically active; the results revealed that the SBA-15@ADMPT led to 23% of product after 12 h and the SBA-15 produced 21% of product after 12 h (entries 6 and 7, respectively). Although the components of the nanocomposite material showed slight catalytic activity, SBA-15@ADMPT/HPA gave the best result in the desired organic synthesis (entry 2). Clearly, grafting the heteropolyacid onto the modified solid material SBA-15@

Table 2 Effect of the catalyst amount for the synthesis of 2-amino-3-cyanopyridine **3a**

Entry	Catalyst	Amount (mg)	Time (h)	Yield (%) ^a
1	SBA-15@ADMPT@HPA	15	2	79
2	SBA-15@ADMPT@HPA	20	2	84
3	SBA-15@ADMPT@HPA	50	2	78
4	SBA-15@ADMPT@HPA	80	2	71
5	$H_5PW_{10}V_2O_{40}$	6.3	8	54
6	SBA-15@ADMPT	20	12	23
7	SBA-15	20	12	21

Reaction conditions: 4-methylbenzaldehyde **1a** (1 mmol), cyclohexanone **2a** (1 mmol), malononitrile (1 mmol), and ammonium acetate (1.5 mmol), ethanol (5 mL), r.t

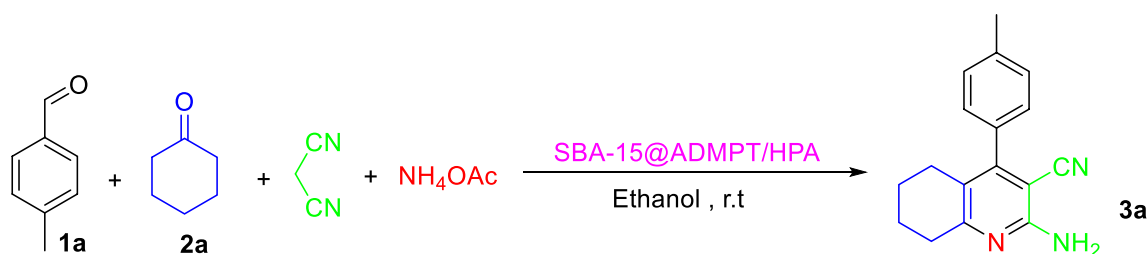
^aIsolated yield based on **1a**

ADMPT drastically increased its catalytic activity toward the organic reaction.

Various solvents such as water, dimethylformamide (DMF), acetonitrile, chloroform, and ethanol were investigated for the model reaction of 4-methylbenzaldehyde, cyclohexanone, malononitrile, and ammonium acetate in the presence of 20 mg of SBA-15@ADMPT/HPA to find the optimum reaction media (Table 3). All reactions were carried out at room temperature. It was found that the best result was obtained in the EtOH as a green solvent (Table 2, entry 1).

Effect of reaction time on the preparation of 2-amino-3-cyanopyridine **3a** in the presence of 20 mg of SBA-15@ADMPT/HPA nanocatalyst was investigated to explore minimum time required to obtain the maximum yield of product. Results summarized in Fig. 7 shows that only 2 h is sufficient to get 84% yield. No obvious increase was detected in the yield after a prolonged reaction time.

To evaluate the generality of the present protocol for the synthesis of 2-amino-3-cyanopyridine **3** and **4**, we investigated the reaction with a wide range of aldehydes carrying either electron-withdrawing, electron-donating, and halogen



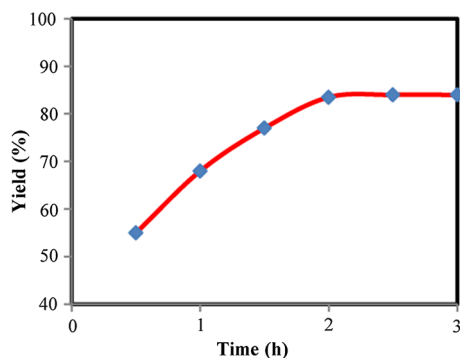
Scheme 4 Model reaction for the synthesis of 2-amino-3-cyanopyridine **3a**

Table 3 Effect of different solvents on the synthesis of 2-amino-3-cyanopyridine **3a** in the presence of SBA-15@ADMPT/HPA

Entry	Solvent	Time	Yield (%) ^a
1	EtOH	2	84
2	H ₂ O	6	Trace
3	DMF	6	Trace
4	CH ₃ CN	6	Trace
5	CHCl ₃	6	Trace
6	–	6	Trace

Reaction conditions are as described below Table 2; 5 ml solvent was used

^aIsolated yield based on **1a**

**Fig. 7** Effect of reaction time on the preparation of 2-amino-3-cyanopyridine **3a**. Reaction conditions are as described below Table 2

groups on the aromatic rings under optimized conditions (Table 4). In general, the reaction proceeded smoothly to give the desired 2-amino-3-cyanopyridine products in high to excellent yields at room temperature and also demonstrated good compatibility with many valuable functional groups such as methoxy, chloro, and bromo substituents. Tolerance to the bromo and chloro functional groups was particularly noteworthy since they are useful for subsequent cross-coupling reactions. From the results displayed in Table 4, it is evident that spatially hindered aldehydes (2,4-dichloro, 2-chloro, and 2,4-dimethoxy substituted) gave the desired products in high yield after 2 h (Table 4, entries 3, 4, 10, and 14). As can be seen from Table 4, the electronic factors seem to have little influence on the reaction since either the electron-donating or the electron-withdrawing groups on the aldehydes ring resulted in the slightly discriminate yields. Methylamine was also used instead of ammonium acetate (NH₄OAc) in the target condensation reaction with 4-methylbenzaldehyde (Table 4 entry 7). Comparison of the results obtained for methylamine and NH₄OAc clearly demonstrated that the NH₄OAc was slightly more reactive toward the condensation reaction than methylamine. 4-methylbenzaldehyde produced 84% yield with NH₄OAc after 2 h

(Table 4, entry 1), whereas methylamine led to 82% yield in 2 h (Table 4, entry 7). All products were characterized by FT-IR and ¹H NMR spectral analysis. To the best of our knowledge, there is not any report of physical properties and spectral data of the **3e**, **3g**, **4c**, **4f**, and **4i** products. The results are summarized in Table 4.

In order to establish that the catalytic activity was generated from the heterogeneous SBA-15@ADMPT/HPA and not from leached heteropolyacid in the reaction mixture, a hot filtration test was carried out. In this technique, the condensation reaction of 4-methylbenzaldehyde (1 mmol), cyclohexanone (1 mmol), malononitrile (1 mmol), and ammonium acetate (1.5 mmol) was performed at room temperature for 60 min in the presence of SBA-15@ADMPT/HPA nanocatalyst (20 mg). In this stage, the yield of the product was 63%. Then, the heterogeneous nanocatalyst was filtered off under hot conditions, and with the filtrate, which was obtained after separation of the nanocatalyst, the condensation reaction was continued for another 30 min at room temperature. But no increase was observed in the product yield after this time. This result clearly demonstrated the heterogeneous nature of the nanocatalyst and no leaching of the heteropolyacid occurred during the reaction.

A major drawback of free heteropolyacid is the separation and recovery of the catalyst when the reaction is completed. Heterogenization of the H₅PW₁₀V₂O₄₀ via anchoring to SBA-15@ADMPT is an attractive strategy, allowing easy separation of the catalyst from the reaction mixture. Moreover, recyclability and reusability of the catalyst reduce amount of wastage and production of wasteful materials. To demonstrate the reusability of the SBA-15@ADMPT/HPA nanocatalyst, it was simply separated from the reaction mixture by filtration and washed with acetone. The catalyst was dried in air and activated in vacuum oven at 80 °C for 2 h. Then, the recycled catalyst was reused in the subsequent fresh reactions. As shown in Fig. 8, there is no significant loss of catalytic activity after five times. Thus, it could be concluded that SBA-15@ADMPT/HPA could be a satisfactory catalyst for this reaction with good reusability and high activity.

Comparison of the catalytic efficiency of SBA-15@ADMPT/HPA nanocatalyst with other literature reported catalysts

In the previous reports, cyclic ketones, such as cycloheptanone and cyclohexanone, are rarely used as starting material to synthesize multisubstituted pyridines, probably because of their low activity. To explore the capability of the present method in comparison with literature methods for the preparation of the title compounds, the reaction of 4-methylbenzaldehyde **1a** with cyclohexanone and 4-methoxybenzaldehyde **1b** with cycloheptanone for the synthesis

Table 4 Synthesis of 2-amino-3-cyanopyridine derivatives **3** and **4** via one-pot, four-component reaction in the presence of SBA-15@ADMPT/HPA nanocatalyst in EtOH at room temperature ^a

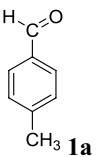
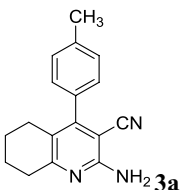
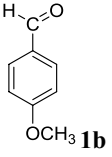
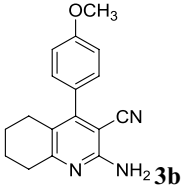
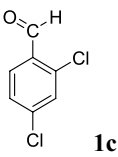
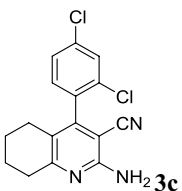
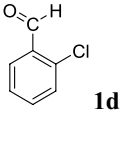
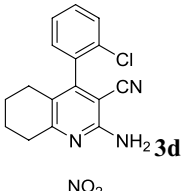
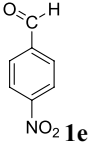
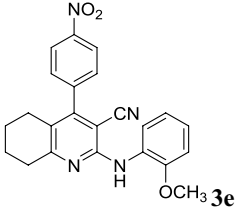
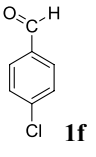
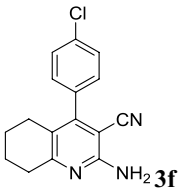
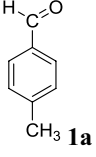
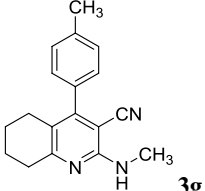
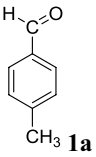
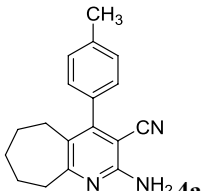
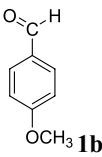
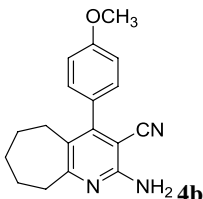
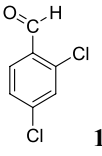
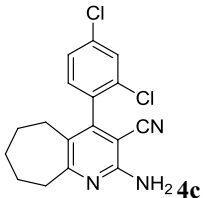
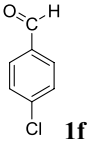
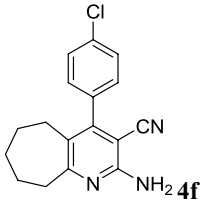
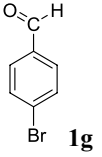
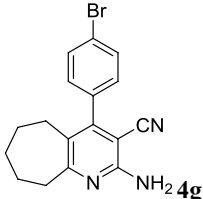
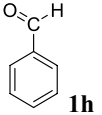
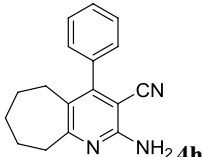
Entry	Aldehyde	Product	Time (h)	Yield (%) ^a	m.p. (°C)	
					Obsd.	Lit.
1			120	84	246–258	248–249 [12]
2			120	97	228–230	226–228 [10]
3			115	85	226–228	225–227 [10]
4			120	83	255–257	257–258 [10]
5			110	77	163–166	Present work
6			120	88	255–257	256–258 [12]
7			120	82	126–129	Present work
8			120	85	230–232	232–233 [45]

Table 4 (continued)

Entry	Aldehyde	Product	Time (h)	Yield (%) ^a	m.p. (°C)	
					Obsd.	Lit.
9	 1b	 4b	120	93	223–225	223–224 [46]
10	 1c	 4c	120	81	245–247	Present work
11	 1f	 4f	120	83	241–243	Present work
12	 1g	 4g	120	91	235–237	236–237 [9]
13	 1h	 4h	120	92	225–227	227–228 [46]

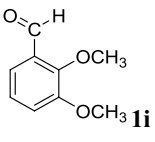
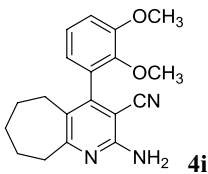
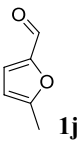
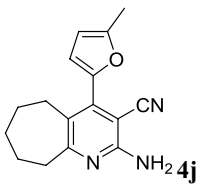
of the corresponding 2-amino-3-cyanopyridine **3a** and **4b** was selected as model reactions and the comparison was in terms of solvent, temperature, reaction time, and percentage yields (Table 5). Obviously, the present new nanohybrid catalyst (SBA-15@ADMPT/HPA) is more effective than other literature reported catalysts.

Proposed reaction pathway for the catalytic system

A proposed mechanism for the SBA-15@ADMPT/HPA-catalyzed formation of 2-amino-3-cyano derivatives is shown in Scheme 5. The formation of 2-amino-3-cyano

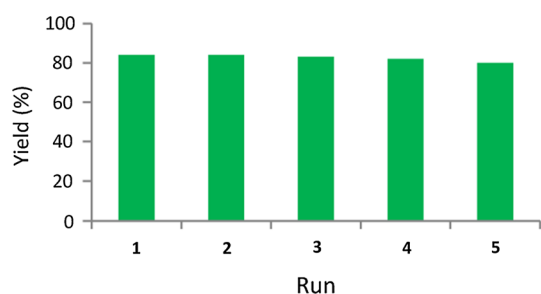
derivatives can be rationalized by the initial formation of arylidene malononitrile (A) as an intermediate via the standard Knoevenagel condensation by the nucleophilic addition of malononitrile to the carbonyl group of the aldehyde which was activated by the SBA-15@ADMPT/HPA nanocatalyst. This is followed by the Michael type addition of cycloheptanone to the activated double bond of the arylidene malononitrile (A). Intramolecular cyclization of enamine B (formed from the reaction of carbonyl group of cycloheptanone and ammonium acetate) by the nucleophilic addition of enamine to the nitrile group which was activated by the nanocatalyst and subsequent

Table 4 (continued)

Entry	Aldehyde	Product	Time (h)	Yield (%) ^a	m.p. (°C)	
					Obsd.	Lit.
14	 1i	 4i	120	79	120–121	Present work
15	 1j	 4j	120	77	162–165	164–166 [47]

Reactions were carried out as described in the experimental section

^aIsolated yields

**Fig. 8** Reusability of SBA-15@ADMPT/HPA nanocatalyst

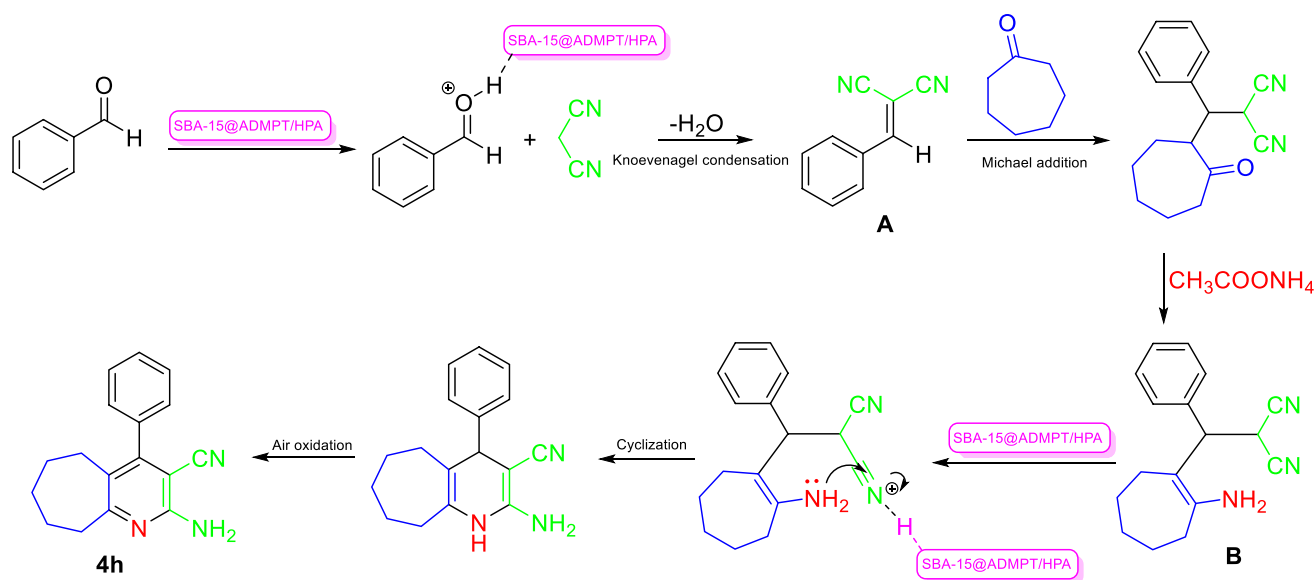
oxidation yielded target product **4** h (Scheme 5). The nanocatalyst with the large specific surface area and good adsorption capacity for organic molecules increases the product yields and reduces the reaction times.

Conclusion

In summary, a new inorganic–organic nanohybrid material SBA-15@triazine/H₅PW₁₀V₂O₄₀ was fabricated from commercially available starting materials and used as an efficient catalyst for the one-pot preparation of 2-amino-3-cyano derivatives from the four-component condensation reaction of aldehydes, cyclic ketones, malononitrile, and ammonium acetate. The catalyst was fully characterized, and the catalytic reactions were carried out in the presence of a catalytic amount of SBA-15@triazine/H₅PW₁₀V₂O₄₀ at room temperature. Furthermore, the catalyst could be successfully recovered and reused at least for five runs without significant loss of activity. Moreover, other advantages such as short reaction times, high product yields, green reaction media, room-temperature operating conditions, and easy work-up procedures make this method an interesting alternative to other methodologies. In general, these advantages highlight this protocol as an attractive and useful methodology,

Table 5 Comparison of the catalytic efficiency of SBA-15@ADMPT/HPA nanocatalyst with other literature reported catalysts for the synthesis of **3a** and **4b**

Entry	Catalyst	R	Product	Solvent	Temp.	Time (h)	Yield (%)	References
1	–	4-CH ₃	3a	Benzene	Reflux	4	74	[45]
2	[bmim]OH	4-CH ₃	3a	[bmim]OH	80 °C	4	83	[10]
3	Fe ₃ O ₄ /cellulose	4-CH ₃	3a	Ethanol	r.t.	3	80	[12]
4	SBA-15@ADMPT/HPA	4-CH ₃	3a	Ethanol	r.t.	2	84	This work
5	–	4-OCH ₃	4b	Benzene	Reflux	4	68	[45]
6	Fe ₃ O ₄ /cellulose	4-OCH ₃	4b	Ethanol	r.t.	3	90	[12]
7	Au/MgO	4-OCH ₃	4b	Ethanol	70 °C	2.5	90	[9]
9	SBA-15@ADMPT/HPA	4-OCH ₃	4b	Ethanol	r.t.	2	93	This work



Scheme 5 Plausible mechanism for the synthesis of **4h**

among the other methods reported in the literature, for the eco-friendly and rapid synthesis of biologically active multistituted pyridines.

Acknowledgements The authors are grateful to the University of Kashan for supporting this work by Grant No. 573600/1.

References

- G.D. Henry, *Tetrahedron* **60**, 6043 (2004)
- E. Kianmehr, M. Ghanbari, M.N. Niri, R. Faramarzi, *J. Comb. Chem.* **12**, 41 (2009)
- A. Maleki, A.A. Jafari, S. Yousefi, *J. Iran. Chem. Soc.* **14**, 1801 (2017)
- E. Ibrahim, G. Elgemeie, M. Abbasi, Y. Abbas, M. Elbadawi, A. Attia, *Nucleosides, Nucleotides Nucleic Acids* **14**, 1415 (1995)
- B.C. May, J.A. Zorn, J. Witkop, J. Sherrill, A.C. Wallace, G. Legname, S.B. Prusiner, F.E. Cohen, *J. Med. Chem.* **50**, 65 (2007)
- T. Murata, M. Shimada, S. Sakakibara, T. Yoshino, H. Kadono, T. Masuda, M. Shimazaki, T. Shintani, K. Fuchikami, K. Sakai, *Bioorg. Med. Chem. Lett.* **13**, 913 (2003)
- J. Deng, T. Sanchez, L.Q. Al-Mawsawi, R. Dayam, R.A. Yunes, A. Garofalo, M.B. Bolger, N. Neamati, *Bioorg. Med. Chem.* **15**, 4985 (2007)
- M. Mantri, O. de Graaf, J. van Veldhoven, A. Göblyös, J.K. von Frijtag Drabbe Künzel, T. Mulder-Krieger, R. Link, H. de Vries, M.W. Beukers, J. Brussee *J. Med. Chem.* **51**, 4449 (2008)
- R. Pagadala, S. Maddila, V. Moodley, W.E. van Zyl, S.B. Jonnalagadda, *Tetrahedron Lett.* **55**, 4006 (2014)
- Y. Wan, R. Yuan, F.-R. Zhang, L.-L. Pang, R. Ma, C.-H. Yue, W. Lin, W. Yin, R.-C. Bo, H. Wu, *Synth. Commun.* **41**, 2997 (2011)
- S. Khaksar, M. Yaghoobi, *J. Fluor. Chem.* **142**, 41 (2012)
- A. Maleki, A.A. Jafari, S. Yousefi, V. Eskandarpour, *C. R. Chim.* **18**, 1307 (2015)
- J. Tang, L. Wang, Y. Yao, L. Zhang, W. Wang, *Tetrahedron Lett.* **52**, 509 (2011)
- M. Thimmaiah, P. Li, S. Regati, B. Chen, J.C.-G. Zhao, *Tetrahedron Lett.* **53**, 4870 (2012)
- I.V. Kozhevnikov, *Chem. Rev.* **98**, 171 (1998)
- V. Brahmkhatri, A. Patel, *Appl. Catal. A* **403**, 161 (2011)
- M. Heravi, S. Sadjadi, *J. Iran. Chem. Soc.* **6**, 1 (2009)
- R. Tayebbe, M. Amini, S. Pouyamanesh, A. Aliakbari, *Dalton Trans.* **44**, 5888 (2015)
- A. Ayati, M.M. Heravi, M. Daraie, B. Tanhaei, F.F. Bamoharram, M. Sillanpaa, *J. Iran. Chem. Soc.* **13**, 2301 (2016)
- G. Marci, E.I. García-López, L. Palmisano, *Eur. J. Inorg. Chem.* **2014**, 21 (2014)
- A. Patel, N. Narkhede, S. Singh, S. Pathan, *Catal. Rev.* **58**, 337 (2016)
- J.P. Arhancet, M.E. Davis, J.S. Merola, B.E. Hanson, *Nature* **339**, 454 (1989)
- D.E. De Vos, P.A. Jacobs, *Catal. Today* **57**, 105 (2000)
- E. Byambajav, Y. Ohtsuka, *Appl. Catal. A* **252**, 193 (2003)
- J. Parmentier, S. Saadhallah, M. Reda, P. Gibot, M. Roux, L. Vidal, C. Vix-Guterl, J. Patarin, *J. Phys. Chem. Solids* **65**, 139 (2004)
- S. Hekmat, S. Balalaie, S. Ramezani, F. Rominger, V.F. Vavsari, H. Kabiri-Fard, *J. Iran. Chem. Soc.* **14**, 833 (2017)
- V.F. Vavsari, G.M. Ziarani, S. Balalaie, A. Latifi, M. Karimi, A. Badiie, *Tetrahedron* **72**, 5420 (2016)
- M. Ghanbari, K. Jadidi, M. Mehrdad, N. Assempour, *Tetrahedron* **72**, 4355 (2016)
- M. Ghanbari, E. Kianmehr, S.K. Behzad, S.W. Ng, *J. Iran. Chem. Soc.* **13**, 7 (2016)
- E. Kianmehr, M. Ghanbari, *Eur. J. Org. Chem.* **2012**, 256 (2012)
- E. Kianmehr, M. Ghanbari, N. Faghhi, F. Rominger, *Tetrahedron Lett.* **53**, 1900 (2012)
- E. Soleimani, M.M. Khodaei, P. Mehrdadi-Nejad, M. Ghanbari, *J. Chem. Res.* **40**, 371 (2016)
- K. Jadidi, R. Ghahremanzadeh, M. Mehrdad, M. Ghanbari, H. Arvin-Nezhad, *Monatshfte für Chemie-Chemical Monthly* **139**, 277 (2008)
- E. Kianmehr, N.S. Zafarghandi, M. Ghanbari, *Mol. Divers.* **17**, 383 (2013)
- G.A. Tsigdinos, C.J. Hallada, *Inorg. Chem.* **7**, 437 (1968)

36. S.K. Behzad, A. Balati, M.M. Amini, M. Ghanbari, *Microchimica Acta* **181**, 1781 (2014)
37. S.K. Behzad, M.M. Amini, A. Balati, M. Ghanbari, O. Sadeghi, *J. Sol-Gel Sci. Technol.* **78**, 446 (2016)
38. D. Zhao, Q. Huo, J. Feng, B.F. Chmelka, G.D. Stucky, *J. Am. Chem. Soc.* **120**, 6024 (1998)
39. H.-J. Kim, Y.-G. Shul, H. Han, *Appl. Catal. A: Gen.* **299**, 46 (2006)
40. D. Zhao, J. Feng, Q. Huo, N. Melosh, G.H. Fredrickson, B.F. Chmelka, G.D. Stucky, *Science* **279**, 548 (1998)
41. R. Tayebee, M.M. Amini, M. Ghadamgahi, M. Armaghan, *J. Mol. Catal. A: Chem.* **366**, 266 (2013)
42. S. Ernst, M. Selle, *Microporous Mesoporous Mater.* **27**, 355 (1999)
43. A. Tarlani, M. Abedini, A. Nemati, M. Khabaz, M.M. Amini, *J. Colloid Interface Sci.* **303**, 32 (2006)
44. R. Tayebee, M.M. Amini, F. Nehzat, O. Sadeghi, M. Armaghan, *J. Mol. Catal. A: Chem.* **366**, 140 (2013)
45. S. Kambe, K. Saito, A. Sakurai, H. Midorikawa, *Synthesis* **1980**, 366 (1980)
46. S. Kankala, R. Pagadala, S. Maddila, C.S. Vasam, S.B. Jonnalagadda, *RSC Adv.* **5**, 105446 (2015)
47. A. Altundas, S. Ayvaz, E. Logoglu, *Med. Chem. Res.* **20**, 1 (2011)